Tip-Induced Orientational Order of Surfactant Micelles on Gold

Hannes C. Schniepp, Dudley A. Saville,† and Ilhan A. Aksay*

Department of Chemical Engineering, Princeton University, Princeton, New Jersey 08544

Received October 7, 2007. In Final Form: November 29, 2007

Using liquid-cell atomic force microscopy, we investigate aqueous solutions of alkyltrimethylammonium halide surfactants at the Au(111) surface. The long, micellar surfactant surface aggregates cover the gold surface completely and exhibit two types of orientational order for chloride and bromide counterions, respectively. We observe lateral forces perpendicular to the scanning direction, which we explain by anisotropic friction between the probe and the oriented micelles. Conversely, we show that these friction forces can be employed to modify the spatial conformation of the micellar adlayer. Where previous methods have failed to provide control over the orientation down to the level of individual micelles, we use this technique to achieve a very high degree of order over more than 100 micelle diameters.

Self-assembly is a promising fabrication technique[1−8] providing very high structural control and order on the nano- to micrometer scale. A major shortcoming of this method, however, is that it is not capable of providing deterministically defined structures at macroscopic length scales[5,6,9,10] because a multitude of domains are formed in an uncontrolled way as a result of the statistical nature of domain nucleation and growth.[5,6,11,12] To overcome this problem, several approaches to guide self-assembly have been suggested and investigated, including crystal-field anisotropy,[5,13,14] topographic surface features,[15−23] physical confinement,[10,16,24−26] shear flow,[16,27−35] magnetic[36,37] and electric[10,38] fields, and electrochemically driven assembly,[39] as well as combinations thereof.[5,10,29]

Nano- and microstructures that are self-assembled from amphiphilic molecules are capable of templating inorganic structures, which is an essential concept of biomineralization.[40,41] Similarly, surfactants are used for the synthetic production of templated silica structures featuring hexagonally packed cylindrical holes with diameters that are tunable between ∼2 and 10 nm.[42] The lack of long-range order is very disadvantageous in this case because it prevents the accessibility and continuity of these channels,[43] which is a prerequisite to their application for molecular separation, catalysis, drug delivery, sensors, and energy storage.[44] Preferred orientation in the templated silica structures has been achieved using shear flow, as demonstrated by X-ray diffraction (XRD),[16,27,28,31] polarized optical microscopy,[28] or by simply analyzing the shapes of the structures grown on a larger scale.[16,28,29] Transmission electron microscopy, however, has revealed that the angular alignment is still far from perfect on the micellar level.[31] One method to provide very strong

* Corresponding author. E-mail: iaksay@princeton.edu.
† Deceased October 4, 2006.

(1) Whitesides, G. M.; Grzybowski, B. *Science* **2002**, *295*, 2418.
(2) Whitesides, G. M.; Mathias, J. P.; Seto, C. T. *Science* **1991**, *254*, 1312.
(3) Glotzer, S. C.; Solomon, M. J.; Kotov, N. A. *AIChE J.* **2004**, *50*, 2978.
(4) Cölfen, H.; Mann, S. *Angew. Chem., Int. Ed.* **2003**, *42*, 2350.
(5) Aksay, I. A.; Trau, M.; Manne, S.; Honma, I.; Yao, N.; Zhou, L.; Fenter, P.; Eisenberger, P. M.; Gruner, S. M. *Science* **1996**, *273*, 892.
(6) Dabbs, D. M.; Aksay, I. A. *Annu. Rev. Phys. Chem.* **2000**, *51*, 601.
(7) Murray, C. B.; Kagan, C. R.; Bawendi, M. G. *Science* **1995**, *270*, 1335.
(8) Winfree, E.; Liu, F. R.; Wenzler, L. A.; Seeman, N. C. *Nature* **1998**, *394*, 539.
(9) Lopinski, G. P.; Wayner, D. D. M.; Wolkow, R. A. *Nature* **2000**, *406*, 48.
(10) Trau, M.; Yao, N.; Kim, E.; Xia, Y.; Whitesides, G. M.; Aksay, I. A. *Nature* **1997**, *390*, 674.
(11) Harrison, C.; Adamson, D. H.; Cheng, Z.; Sebastian, J. M.; Sethuraman, S.; Huse, D. A.; Register, R. A.; Chaikin, P. M. *Science* **2000**, *290*, 1558.
(12) Harrison, C.; Angelescu, D. E.; Trawick, M.; Cheng, Z.; Huse, D. A.; Chaikin, P. M.; Vega, D. A.; Sebastian, J. M.; Register, R. A.; Adamson, D. H. *Europhys. Lett.* **2004**, *67*, 800.
(13) Saville, D. A.; Chun, J.; Li, J.-L.; Schniepp, H. C.; Car, R.; Aksay, I. A. *Phys. Rev. Lett.* **2006**, *96*, 018301.
(14) Chun, J.; Li, J.-L.; Car, R.; Aksay, I. A.; Saville, D. A. *J. Phys. Chem. B* **2006**, *110*, 16624.
(15) Miyata, H.; Kuroda, K. *Adv. Mater.* **1999**, *11*, 1448.
(16) Miyata, H.; Kuroda, K. *Chem. Mater.* **1999**, *11*, 1609.
(17) Hahn, J.; Webber, S. E. *Langmuir* **2003**, *19*, 3098.
(18) Hahn, J.; Webber, S. E. *Langmuir* **2004**, *20*, 1489.
(19) Stoykovich, M. P.; Muller, M.; Kim, S. O.; Solak, H. H.; Edwards, E. W.; de Pablo, J. J.; Nealey, P. F. *Science* **2005**, *308*, 1442.
(20) Stoykovich, M. P.; Edwards, E. W.; Solak, H. H.; Nealey, P. F. *Phys. Rev. Lett.* **2006**, *97*, 147802.
(21) Chuang, V. P.; Cheng, J. Y.; Savas, T. A.; Ross, C. A. *Nano Lett.* **2006**, *6*, 2332.
(22) Edwards, E. W.; Muller, M.; Stoykovich, M. P.; Solak, H. H.; de Pablo, J. J.; Nealey, P. F. *Macromolecules* **2007**, *40*, 90.
(23) Crnogorac, F.; Witte, D. J.; Xia, Q.; Rajendran, B.; Pickard, D. S.; Liu, Z.; Mehta, A.; Sharma, S.; Yasseri, A.; Kamins, T. I.; Chou, S. Y.; Pease, R. F. W. *Microelectron. Eng.* **2007**, *84*, 891.
(24) Yang, P.; Deng, T.; Zhao, D.; Feng, P.; Pine, D.; Chmelka, B. F.; Whitesides, G. M.; Stucky, G. D. *Science* **1998**, *282*, 2244.
(25) Yamaguchi, A.; Uejo, F.; Yoda, T.; Uchida, T.; Tanamura, Y.; Yamashita, T.; Teramae, N. *Nat. Mater.* **2004**, *3*, 337.
(26) Wu, Y.; Cheng, G.; Katsov, K.; Sides, S. W.; Wang, J.; Tang, J.; Fredrickson, G. H.; Moskovits, M.; Stucky, G. D. *Nat. Mater.* **2004**, *3*, 816.
(27) Melosh, N. A.; Davidson, P.; Feng, P.; Pine, D. J.; Chmelka, B. F. *J. Am. Chem. Soc.* **2001**, *123*, 1240.
(28) Hillhouse, H. W.; van Egmond, J. W.; Tsapatsis, M.; Hanson, J. C.; Larese, J. Z. *Chem. Mater.* **2000**, *12*, 2888.
(29) Hillhouse, H. W.; Okubo, T.; van Egmond, J. W.; Tsapatsis, M. *Chem. Mater.* **1997**, *9*, 1505.
(30) Edler, K. J.; Reynolds, P. A.; Brown, A. S.; Slawecki, T. M.; White, J. W. *J. Chem. Soc., Faraday Trans.* **1998**, *94*, 1287.
(31) Kim, W. J.; Yang, S. M. *Chem. Mater.* **2000**, *12*, 3227.
(32) Angelescu, D. E.; Waller, J. H.; Register, R. A.; Chaikin, P. M. *Adv. Mater.* **2005**, *17*, 1878.
(33) Vega, D. A.; Harrison, C. K.; Angelescu, D. E.; Trawick, M. L.; Huse, D. A.; Chaikin, P. M.; Register, R. A. *Phys. Rev. E* **2005**, *71*, 061803.
(34) Wu, M. W.; Register, R. A.; Chaikin, P. M. *Phys. Rev. E* **2006**, *74*, 040801.
(35) Pelletier, V.; Asakawa, K.; Wu, M. S.; Adamson, D. H.; Register, R. A.; Chaikin, P. M. *Appl. Phys. Lett.* **2006**, *88*, 211114.
(36) Tolbert, S. H.; Firouzi, A.; Stucky, G. D.; Chmelka, B. F. *Science* **1997**, *278*, 264.
(37) Firouzi, A.; Schaefer, D. J.; Tolbert, S. H.; Stucky, G. D.; Chmelka, B. F. *J. Am. Chem. Soc.* **1997**, *119*, 9466.
(38) Ku, A. Y.; Saville, D. A.; Aksay, I. A. *Langmuir* **2007**, *23*, 8156.
(39) Walcarius, A.; Sibottier, E.; Etienne, M.; Ghanbaja, J. *Nat. Mater.* **2007**, *6*, 602.
(40) Lowenstam, H. A.; Weiner, S. *On Biomineralization*; Oxford University Press: Oxford, U.K., 1989.
(41) *Biomineralization: Chemical and Biochemical Perspectives*; Mann, S., Webb, J., Williams, R. J. P., Eds.; VCH Press: New York, 1989.
(42) Kresge, C. T.; Leonowicz, M. E.; Roth, W. J.; Vartuli, J. C.; Beck, J. S. *Nature* **1992**, *359*, 710.
(43) Yao, N.; Ku, A. Y.; Nakagawa, N.; Lee, T.; Saville, D. A.; Aksay, I. A. *Chem. Mater.* **2000**, *12*, 1536.
(44) Lu, G. Q.; Zhao, X. S. *Nanoporous Materials, Science and Engineering*; Imperial College Press: London, 2004.

10.1021/la703096a CCC: $40.75
Published on Web 01/09/2008

angular guidance is crystal-field anisotropy provided by a templating surface,[5,13,14] which strictly locks surfactant micelles that are adsorbed on certain surfaces into orientations dictated by the surface lattice.[45−54] However, the surfaces for which this phenomenon has been observed so far−graphite(0001),[5,13,45−51] Au(111),[52−54] and molybdenum disulfide(0001)[46]−all have three equivalent symmetry axes. Therefore, there is still more than one preferred direction, and the desired macroscopically unique orientation is not readily achieved. In this letter, we show that an effective way of guiding self-assembly is based on crystal-field anisotropy combined with a new method for removing this remaining degree of disorder by guiding the micelles with the tip of an atomic force microscope (AFM).

Our experimental work was conducted on Au(111) surfaces, which have been shown to cause the lattice-induced self-assembly of surfactants such as sodium dodecyl sulfate (SDS)[52−54] and hexadecyltrimethylammonium hydroxide (C_{16}TAOH).[52] However, not all surfactants exhibit the same behavior on Au(111). Jaschke et al. have shown that the orientation of tetradecyltrimethylammonium bromide (C_{14}TAB) aggregates on Au(111) is not determined by the substrate lattice; instead, the C_{14}TAB micelles align with topographic features on the surface.[52] The authors suggested that the specific interaction between the bromide counterions and the gold surface is related to this behavior: if bromide adsorption is particularly strong at surface defects, then they become negatively charged, thus attracting the cationic surfactant. According to this rationale, the first adsorbed surfactant follows topographic features on the surface, directing the orientational order of the micellar structures following later. Our experimental results with AFM imaging reported here reveal that this behavior is quite specific to the bromide counterion. With hexadecyltrimethylammonium chloride (C_{16}TAC), where only the bromide is replaced by another halide (chloride), the lattice-induced orientation is recovered. Therefore, simply by changing the counterion, the orientational recognition of the substrate lattice by the surfactant aggregates can be switched on or off.

The main goal of this work−controlling the surfactant orientation on a surface−is achieved by manipulating the micelles using the probe of an AFM. Using the AFM probe, we are able to change the orientation of C_{16}TAC surfactant aggregates in a controlled fashion. With this method, we force all micelles in an area that is more than 100 micelle diameters wide into a single direction. Applying the same technique to C_{14}TAB, which does not exhibit lattice-induced anisotropic adsorption on Au(111), we did not succeed in increasing the degree of order of the surface micelles substantially. Our results thus suggest that a substrate providing crystal-field anisotropy is necessary to achieve tip-induced ordering of surfactant surface aggregates.

For the analysis of the tip-induced micelle orientation, we use AFM in a new way to determine both the micellar structure of a C_{16}TAC boundary layer on Au(111) as well as the friction between the tip and the surface, simultaneously and with nanometer resolution. We find that the friction varies locally and is determined by the orientation of the micelles. Friction is minimal when the tip runs parallel to the micelles. We hypothesize that this friction anisotropy is the origin of the observed tip-induced reorientation of the surface micelles. Similar friction anisotropy has been observed for liquid crystals but not for molecularly thin layers of surfactants.[55,56] Traditionally, the friction properties of boundary layers have been studied using the surface force apparatus (SFA);[57−60] the addition of optical techniques to the SFA have allowed the detection of orientational anisotropy of the lubricant.[56] However, the area probed by both the SFA and far-field optical techniques in general is orders of magnitude larger than molecular dimensions and thus averages over thousands of molecular units. Information about the molecular-scale organization or even structural inhomogeneities of the lubricant at larger length scales[61−63] is thus not accessible to such tools. Our results emphasize the importance of the molecular-scale conformation of a surfactant lubricant in aqueous environments. Lubrication under such conditions was recently studied[64] because of its importance in biological systems[65−67] as well as the potential for technical applications.[68,69] For the development of optimized lubricants, we thus propose the consideration of lubricant organization at molecular dimensions.

Experimental Section

Preparation of Samples and Solutions. Atomically smooth gold surfaces were prepared by evaporating a 100-nm-thick gold film directly onto unheated, freshly cleaved mica substrates using a Denton V-502A (Denton Vacuum, Moorestown, NJ) electron beam evaporator. The base pressure before evaporation was below 10^{-6} mbar, and the deposition rate was 0.3 nm/s. The gold surfaces were then annealed in a hydrogen flame using a National 3H stainless steel hydrogen torch with an OX-3 tip (Premier Industries, Blaine, MN). The hydrogen pressure was 400 mbar, and the torch regulator was adjusted to yield a flame about 7 cm long. The mica sheets were held in the flame for about 10 s at a distance of about 5 cm from the torch tip. We confirmed that the (111) planes were oriented parallel to the substrate surface by X-ray diffraction characterization (Rigaku Miniflex diffractometer, The Woodlands, TX) and atomic-resolution AFM lattice scans. The annealed samples were used within minutes after the annealing process to reduce contamination from air as much as possible.

The C_{14}TAB solutions were prepared by dissolving C_{14}TAB powder (99% grade, Sigma-Aldrich, St. Louis, MO) in water deionized using a Picopure 2 UV Plus system (Hydro Service and Supplies, Inc., Durham, NC), featuring a resistivity of 18 MΩ cm. Solutions of C_{16}TAC were obtained by diluting a 25 wt % aqueous C_{16}TAC solution (purum grade, Sigma-Aldrich, St. Louis, MO) with deionized water. The pH values of the surfactant solutions were not adjusted further.

(45) Manne, S.; Cleveland, J. P.; Gaub, H. E.; Stucky, G. D.; Hansma, P. K. *Langmuir* **1994**, *10*, 4409.
(46) Manne, S.; Gaub, H. E. *Science* **1995**, *270*, 1480.
(47) Patrick, H. N.; Warr, G. G.; Manne, S.; Aksay, I. A. *Langmuir* **1997**, *13*, 4349.
(48) Manne, S.; Schäffer, T. E.; Huo, Q.; Hansma, P. K.; Morse, D. E.; Stucky, G. D.; Aksay, I. A. *Langmuir* **1997**, *13*, 6382.
(49) Ducker, W. A.; Grant, L. M. *J. Phys. Chem.* **1996**, *100*, 11507.
(50) Grant, L. M.; Tiberg, F.; Ducker, W. A. *J. Phys. Chem. B* **1998**, *102*, 4288.
(51) Schniepp, H. C.; Saville, D. A.; Aksay, I. A. *J. Am. Chem. Soc.* **2006**, *128*, 12378.
(52) Jaschke, M.; Butt, H.-J.; Gaub, H. E.; Manne, S. *Langmuir* **1997**, *13*, 1381.
(53) Burgess, I.; Jeffrey, C. A.; Cai, X.; Szymanski, G.; Galus, Z.; Lipkowski, J. *Langmuir* **1999**, *15*, 2607.
(54) Schniepp, H. C.; Shum, H. C.; Saville, D. A.; Aksay, I. A. *J. Phys. Chem. B* **2007**, *111*, 8708.
(55) Janik, J.; Tadmor, R.; Klein, J. *Langmuir* **2001**, *17*, 5476.
(56) Nakano, K. *Tribol. Lett.* **2003**, *14*, 17.
(57) Israelachvili, J. N.; Adams, G. E. *J. Chem. Soc., Faraday Trans.* **1978**, *74*, 975.
(58) Yoshizawa, H.; Chen, Y. L.; Israelachvili, J. *J. Phys. Chem.* **1993**, *97*, 4128.
(59) Yoshizawa, H.; Israelachvili, J. *J. Phys. Chem.* **1993**, *97*, 11300.
(60) Bhushan, B.; Israelachvili, J. N.; Landman, U. *Nature* **1995**, *374*, 607.
(61) Wanless, E. J.; Ducker, W. A. *J. Phys. Chem.* **1996**, *100*, 3207.
(62) Perkin, S.; Kampf, N.; Klein, J. *Phys. Rev. Lett.* **2006**, *96*, 038301.
(63) Perkin, S.; Kampf, N.; Klein, J. *J. Phys. Chem. B* **2005**, *109*, 3832.
(64) Briscoe, W. H.; Titmuss, S.; Tiberg, F.; Thomas, R. K.; McGillivray, D. J.; Klein, J. *Nature* **2006**, *444*, 191.
(65) Sarma, A. V.; Powell, G. L.; LaBerge, M. *J. Orthop. Res.* **2001**, *19*, 671.
(66) Hills, B. A. *Proc. Inst. Mech. Eng. H* **2000**, *214*, 83.
(67) Klein, J. *Proc. Inst. Mech. Eng. J* **2006**, *220*, 691.
(68) Sulek, M. W.; Wasilewski, T. *Wear* **2006**, *260*, 193.
(69) Bu, K.-H.; Moudgil, B. M. *J. Electrochem. Soc.* **2007**, *154*, H631.

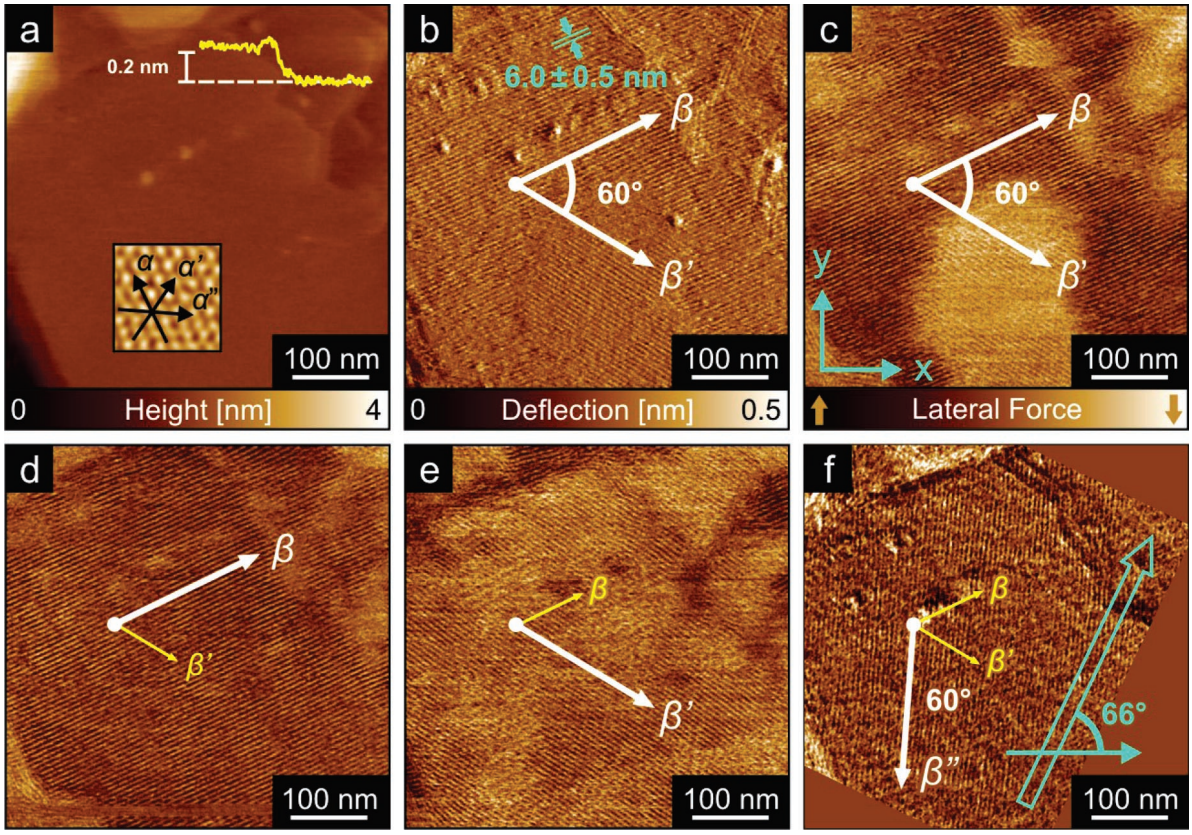

Figure 1. Series of AFM scans showing exactly the same area of the sample at different stages. (a) Topography image showing the investigated area of the Au(111) substrate (insets: topography section across a single atomic step and high-resolution lattice image). (b) Low-force deflection image revealing the surface micelles and their orientation. (c−e) Series of lateral force images showing the C_{16}TAC surface micelles in two different orientations β and β' (with the orientations present in each image indicated by white arrows). (f) Deflection image featuring a micelle orientation in the third direction β''. In this image, the fast scanning direction (indicated by a turquoise, hollow arrow) was not in the x direction but had an angle of 66° relative to the x axis.

Atomic Force Microscopy. All images were acquired in a liquid environment using a commercial MultiMode AFM (Veeco, Santa Barbara, CA) with a NanoScope IIIa controller (software version v5.12r5) equipped with an FC-type contact-mode liquid cell. The AFM piezo scanner was calibrated using a 3D reference silicon grating (Veeco, part number 498-000-026) with a 10 μm lateral pitch and a step height of 100 nm. Cantilevers were NP-S-type (Veeco) oxide-sharpened silicon nitride tips with a reflective gold coating on the back side and a nominal spring constant and tip radius of curvature of 0.06 N/m and 20 nm, respectively. The tips were cleaned in an ozone chamber (UVOCS, Montgomeryville, PA) for 60 min prior to the experiment. The fluid cell (volume 0.5 mL) was flushed with 5 mL of deionized water and left for 1 h to reach thermal equilibrium. Surfactant solutions were then added, and imaging was started.

All imaging was performed in static mode using different force set points and line frequencies of 2−7 Hz. The highest possible integral and proportional gains (typically ∼5) were used to obtain the most accurate representation of the sample. Imaging of micellar aggregates was performed at low force set points in the precontact regime (previously described as double-layer repulsion[45,70] or soft contact[46] imaging modes). The samples were therefore approached with the smallest possible force set point. Once the tip was within a few nanometers of the surface, the force set point was optimized for the best contrast in the signal of interest (topography/deflection or cantilever torsion). To image the topography of the substrate below the surfactant aggregate layer, the force set point was increased until direct contact between the tip and substrate was established.

(70) Senden, T. J.; Drummond, C. J.; Kekicheff, P. *Langmuir* **1994**, *10*, 358.

Results and Discussion

In the following sections, we first establish the structural properties of C_{16}TAC aggregates at the solution−Au(111) interface. Then we demonstrate that the oriented, rodlike C_{16}TAC surface micelles exert orientation-dependent frictional forces on the AFM probe. We show that, as a consequence of this frictional force dependence, tip motion can affect the orientational order of C_{16}TAC micelles in a deterministic way. Finally, we show experimental results for the reorientation of C_{14}TAB micelles, discuss the differences between the C_{14}TAB and C_{16}TAC surfactants, and introduce our suggested mechanism for reorientation.

Orientational Order of C_{16}TAC Micelles on Gold. A series of AFM scans on Au(111) in a 10 mM C_{16}TAC solution were conducted. Figure 1a was taken at a force set point of ∼5 nN. Under such conditions, the surfactant surface aggregates are displaced, and the tip establishes firm contact with the surface.[5,47,51] High-magnification images taken at this force set point reveal the substrate lattice as shown in the inset, with black arrows highlighting the α, α′, and α″ directions corresponding to the $\langle 1\bar{1}0 \rangle$ axes of the (111) plane. This confirms the complete displacement of the surfactant aggregates, and Figure 1a thus represents the topography of the substrate. The cross section overlaid in the top part of Figure 1a features the topography along the white dashed line and leads across a step. The height of this step, which is slightly greater than 200 pm, is in agreement with the expected step height of 235 pm for a single atomic step

on Au(111).[71] Before and after the step, the cross section shows topography variations of as little as ~20 pm, indicating that the large, flat area in the center is atomically smooth, except for a few pointlike elevated defects. The low-force image shown in Figure 1b (deflection signal) was taken in exactly the same sample area; the area can be identified by the corresponding appearance of the steps in the corners and the defects in the center of Figure 1a,b (Supporting Information). The surface shown in Figure 1b is completely covered with long surfactant micelles; the center-to-center spacing of the micelles is (6.0 ± 0.5) nm. Almost all of the C_{16}TAC micelles shown in Figure 1b are perfectly straight, and they are strictly oriented in one of two distinct directions β or β', perpendicular to the crystal axes α and α' of the gold surface. These findings are very similar to what has been reported for the orientational order of SDS[52−54] and C_{16}TAOH micelles on Au(111).[52] However, they deviate significantly from the published results of C_{14}TAB on Au(111), where the micelle orientation is not restricted to preferred orientations dictated by the lattice.

The particular behavior of C_{14}TAB on Au(111) has been rationalized by specific gold−bromide interactions.[52] Because chloride is chemically very similar to bromide, it thus comes as a surprise that C_{16}TAC behaves similarly to C_{16}TAOH but differently from C_{14}TAB. However, there are at least two differences between the interactions of the two halides with gold: the two kinds of ions form different lattice structures on Au(111),[72] and bromide ion adsorbs in higher quantities on Au(111) for a given surface potential.[73−75] The latter is in line with recent measurements by Kawasaki et al.,[76] who found that the surface coverage of C_{16}TAB on Au(111) is higher with respect to C_{16}TAC (203 ± 20 ng/cm^{-2} and 150 ± 20 ng/cm^{-2}, respectively).

Anisotropy of Lateral Forces. The data shown in Figure 1c represent the cantilever torsion induced by lateral forces and correspond to the simultaneously recorded deflection signal depicted in Figure 1b. The surface micelles are clearly visible in the torsion signal, with a contrast that is even stronger than in the topography (not shown) or deflection (Figure 1b) signals. The fact that we see the micelles in the topography and deflection signals confirms that we are operating in the precontact regime, where electrostatic[45,70] and/or steric[46] forces prevent the AFM probe from establishing contact with the substrate. Previously, it was suggested that the tip glides in a virtually frictionless manner across the surface in this precontact regime.[70] In contrast, we measure a significant torsion signal in this regime. The corresponding lateral forces may be caused by steric and/or electrostatic interactions between the tip and the micellar adlayer. Being able to recognize the micelles in the cantilever torsion signal implies that every micelle gives rise to a lateral force between the tip and the surface as the tip glides across the surfactant-populated surface. In some cases, we even observed a micellar torsion signal when the deflection contrast had vanished completely. This excludes crosstalk from cantilever deflection and demonstrates that the torsion is real.

Figure 1c also shows two patches with different micelle orientations. Not only does each patch show a modulation of the torsion signal induced by the micelles, but there is also a systematic difference in the average torsion between patches of different orientations: the patch in the lower center of the image (micelles with β' orientation) is brighter than the surrounding area (micelles with β orientation). Note that the area in question is virtually topography-free, as a comparison with Figure 1a shows. The contrast can therefore be induced only by a difference in micelle orientation. The dependence of the torsion on the micelle orientation can be explained as follows. The cantilever orientation in all AFM images shown in Figure 1 was parallel to the *x* axis of the images (indicated in Figure 1c). The fast scanning direction in Figure 1c was parallel to the *x* axis as well. Because cantilever torsion is induced by lateral forces perpendicular to the cantilever orientation, the colors in Figure 1c represent forces parallel to the *y* axis. This means that the tip-scanning motion of Figure 1c in the *x* direction induces a lateral force in the *y* direction. An analysis of the sign of the torsion shows that when the tip moves from left to right it is subject to lateral forces in the positive *y* direction (pointing to the top of Figure 1c) on micelle patches with β orientation. Correspondingly, a lateral force in the negative *y* direction is induced when the tip moves over a patch in the β' direction. Our explanation for this phenomenon is that it is energetically favorable for the tip to run parallel to the micelles. Because the micelle orientation and the fast scanning direction are not parallel, this can be achieved only by a lateral tip offset, inducing cantilever torsion. At equilibrium, the torsional energy is equivalent to the energetic advantage of running parallel to the micelles.

It is likely that this force not only affects the torsion of the tip but also has an influence on the spatial conformation of the micelles. In the following section, we demonstrate that it is actually possible to change the orientation of surface micelles using the AFM probe. We suspect that this is due to the anisotropic friction between the probe and the micelles.

Tip-Induced Orientation of C_{16}TAC Micelles. At this stage of the experiment, we imaged the area shown in Figure 1c several times with the fast scanning direction oriented in the β direction and with an increased force set point so that contact between the tip and the substrate was established. Then, we acquired Figure 1d using identical imaging parameters than we used to produce Figure 1c. Note that the substrate defects in the corners of Figure 1c,d appear at the same position, confirming that the two images represent the same sample area (Supporting Information). However, now all micelles in the imaged area are pointing in the β direction (Figure 1d), including the area that previously showed the β' orientation. Similarly, by scanning the tip along the β' direction for several images at increased force, we were able to orient the entire scanning area in the β' direction, as shown in Figure 1e. Note that Figure 1d (β orientation) is on average darker than Figure 1e (β' orientation), which is consistent with the orientation-dependent lateral forces observed in Figure 1c.

Finally, we applied the same procedure to the β'' axis, which we expected to be the third preferred micelle orientation because it is perpendicular to the α'' axis of the gold lattice. After scanning the sample at high force in the β'' direction to orient the micelles, the resultant surfactant distribution was imaged using a fast scanning direction at an angle of about 66° relative to the *x* axis (Figure 1f; scanning direction indicated by the hollow, turquoise arrow). To compensate for the changed fast scanning direction, the image was rotated so that Figure 1f represents exactly the same sample area as Figure 1a−e. In Figure 1f, we show the deflection signal in order to visualize the micelles because the cantilever torsion signal in this scan was weak. We rationalize

(71) Chidsey, C. E. D.; Loiacono, D. N.; Sleator, T.; Nakahara, S. *Surf. Sci.* **1988**, *200*, 45.
(72) Magnussen, O. M. *Chem. Rev.* **2002**, *102*, 679.
(73) Shi, Z. C.; Lipkowski, J. *J. Electroanal. Chem.* **1996**, *403*, 225.
(74) Shi, Z. C.; Lipkowski, J.; Mirwald, S.; Pettinger, B. *J. Chem. Soc., Faraday Trans.* **1996**, *92*, 3737.
(75) Lipkowski, J.; Shi, Z. C.; Chen, A. C.; Pettinger, B.; Bilger, C. *Electrochim. Acta* **1998**, *43*, 2875.
(76) Kawasaki, H.; Nishimura, K.; Arakawa, R. *J. Phys. Chem. C* **2007**, *111*, 2683.

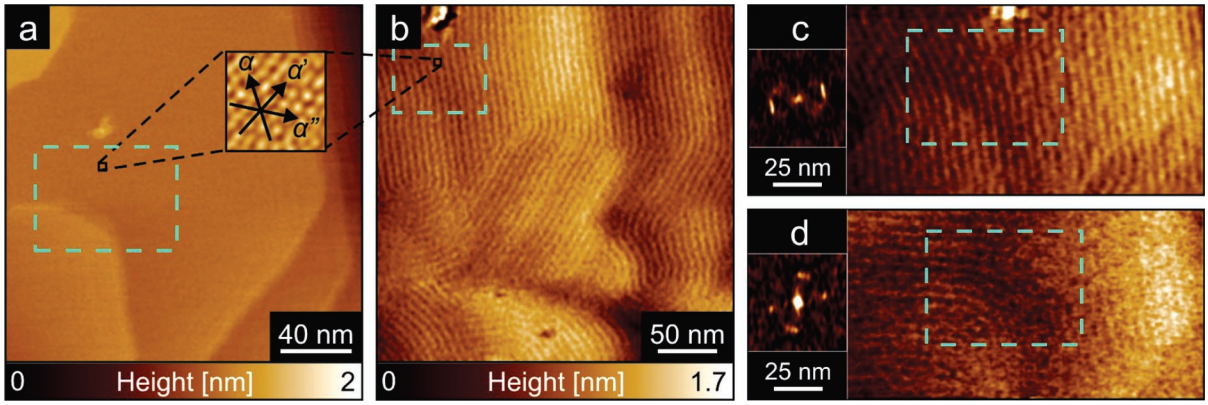

Figure 2. (a) Topography image of a 10 mM C_{14}TAB solution on gold, taken at a high force set point, showing the atomic steps of the substrate (inset: high-resolution lattice image of Au(111) with symmetry axes α, α′, and α″). (b) The same sample area imaged at low force, revealing the surface micelles. (c, d) Topography images showing the C_{14}TAB-covered gold surface before and after reorientation (insets: Fourier transforms of the images). The turquoise rectangle indicates corresponding areas in all scans.

the weak torsion signal as follows. As concluded above, scanning the tip across surfactant surface micelles at an angle induces lateral forces perpendicular to the scanning direction. From these lateral forces, only the component perpendicular to the cantilever orientation induces torsion. In Figure 1c−e, the scanning direction was parallel to the cantilever; the lateral forces thus contribute to the torsion in full. In contrast, in Figure 1f, the scanning direction was oriented at an angle of 66° relative to the cantilever so that only a fraction of cos 66° ≈ 0.4 of the induced lateral forces lead to cantilever torsion.

We were not able to align the micelles along directions other than one of the three preferred directions β, β', or β'' by using a different fast scanning direction φ. After such attempts, we usually found the micelles oriented along the preferred direction that had the smallest angle with the employed fast scanning direction. Even when we were scanning the micelle distribution shown in Figure 1f (β'' orientation) at the lowest possible force set point with the scanning direction parallel to the x axis (0°), this caused a small area to reorient in the β or β' direction. Hence, the tip has a small influence on the micelle orientation, even if it is scanned at the lowest possible force set point. It is not surprising that some parts of the area that was initially completely in β'' orientation are converted to orientation β or β' because they make a smaller angle with the 0° scanning direction.

It has been shown that micellar aggregates at the solid−liquid interface can undergo dynamic reorganization.[13] It is thus possible that the C_{16}TAC aggregates that have been oriented by the AFM probe will reorient and point in a different direction after some time. It would be interesting to know the characteristic times for such a dynamic reorientation process. We have not yet addressed this problem, which may be the subject of a future study. From our data, we can conclude that micelles oriented by the probe can be imaged subsequently several times without losing their orientation, corresponding to a time scale of a few minutes.

Tip-Induced Orientation of C_{14}TAB Micelles. For C_{14}TAB on Au(111), we were able to reproduce the results of Jaschke et al.[52] Figure 2a shows a high-force AFM topography image, taken in a 10 mM C_{14}TAB solution, of the Au(111) surface and its lattice orientation (inset). Figure 2b shows the low-force topography image of the same area of the sample, with a small lateral offset and a smaller magnification. Here, the gold surface is completely covered with elongated micelles. Neighboring micelles often run parallel but do not exhibit a fixed orientation with respect to the lattice symmetry axes. Instead, they typically align with the topography steps of the substrate and even follow them around turns, continuously changing direction, exactly as observed by Jaschke et al.[52] To rule out that the difference in orientational order between C_{14}TAB and C_{16}TAC is due to the small difference in the alkyl chain length (14 vs 16 carbon atoms), we also imaged Au(111) in a 10 mM solution of C_{16}TAB and found virtually identical morphology of the micellar adlayer to that of C_{14}TAB. This is the ultimate confirmation that all structural differences between aggregates of C_{14}TAB and C_{16}TAC are due to the different counterions.

Finally, we tried reorienting the C_{14}TAB micelles by applying exactly the same procedure as for C_{16}TAC. Figure 2c,d shows topography images of the same area before and after such a reorientation attempt. These scans were performed on the same sample featured in Figure 2a, on the large terrace in the center of Figure 2a. The lattice orientation in Figure 2c,d is thus the same as shown in the inset of Figure 2a. The micelles in Figure 2c initially show a relatively narrow distribution of angles, approximately in the y direction. In the Fourier transform of the image (inset), this is represented by two elongated dots left and right of the center. Then, the area was scanned using an increased force set point, keeping the fast scanning direction in the x direction. The following low-force scan (Figure 2d) shows that the micelles in the left part of the image have indeed been reoriented, now approximately parallel to the x axis, representing the fast scanning direction during high-force imaging. This is also evident in the Fourier transform of the image: the spot representing the area in the y orientation (right half of Figure 2d) is weaker and narrower with respect to the Fourier transform of Figure 2c; a new pair of spots above and below the center of the transform represents the area that is now oriented approximately parallel to the x axis. Comparison with the substrate lattice orientation (inset of Figure 2a) shows that the new micelle orientation is not related to any of the lattice symmetry axes. In general, it was much more difficult to achieve the reorientation of C_{14}TAB micelles in comparison to C_{16}TAC. For C_{14}TAB, we observed a change in orientation in only a small fraction of the area that was scanned at a high force. For C_{16}TAC, in contrast, we were easily able to change the micelle orientation over the entire area shown in Figure 1.

The fact that micelle orientation is achieved more easily for the surfactant C_{16}TAC that exhibits lattice-dictated orientation of the adsorbed micelles than for the surfactant C_{14}TAB that does not show strongly preferred orientations can be explained as follows. As concluded above, the energy is minimized if the surfactant micelles under or close to the scanning tip are oriented parallel to the tip-scanning direction. We thus suspect that the micelles are actually reoriented in a small area in the vicinity of

the tip during the scanning process. This small area has an interface with the surrounding area of different micelle orientation. Forming this interface between patches of different micelle orientations comes at an energy cost. Unless the micelle orientation in the small area is energetically favorable, the small area will not be stable: minimization of the described interfacial energy will ultimately annihilate the small area. In the case of C_{16}TAC where certain angles of orientation come with energy benefits, this annihilation process may be slower than the creation of a new area of the same orientation through the AFM probe so that finally an entire patch can be converted to another stable orientation. Because C_{14}TAB micelles do not exhibit a specific orientation with respect to the lattice symmetry axes, the energy benefits of orienting micelles perpendicular to the $\alpha/\alpha'/\alpha''$ orientations are much lower that for C_{16}TAC, making this reorientation process much less likely.

Conclusions

We demonstrated that the C_{14}TAB and C_{16}TAC micelles exhibit a substantial difference in their orientational order on Au(111). C_{14}TAB (and C_{16}TAB) micelles line up with the topographic features of the substrate, whereas C_{16}TAC micelles are strictly aligned perpendicular to the symmetry axes of the Au(111) surface. When we scan an AFM probe across a layer of oriented surface micelles, we observe a lateral force perpendicular to the scanning direction. We attribute this force to anisotropic friction between the probe and the oriented micelles; friction is minimal when the tip is moved parallel to the micelles.

These lateral forces also have an influence on the spatial conformation of the micelles: by scanning the AFM probe across the surface at an increased force set point, the orientation of micelles is modified. For C_{16}TAC, we were able to convert all micelles in the investigated area completely into any of three preferred directions dictated by the gold lattice. For C_{14}TAB, it was rather difficult to modify micelle orientation at all; we achieved it in only a small fraction of the processed area. We hypothesize that surfactant−substrate combinations for which the surface micelles exhibit preferred adsorption angles are easier to reorient because the small areas in which micelle orientation is changed by the probe are more stable.

For C_{16}TAC, we have produced areas of more than 100 micelle diameters in size, in which the orientation is perfect for every micelle within the precision of measurement of our microscope. This approach removes the randomness in orientation between several independently formed micellar patches with different orientations and brings about complete control over orientational order. This is especially interesting because surface micelles can serve as a template for volume structures grown on top of them.[5]

Acknowledgment. We thank Caroline M. Murira for assistance with the preparation of the gold films. Financial support from ARO/MURI under grant no. W911NF-04-1-0170 is greatly appreciated.

Supporting Information Available: Information on the relative position of the imaged areas shown in Figure 1. This material is available free of charge via the Internet at http://pubs.acs.org.

LA703096A